Chapter 1
RTD FLUXGATE MAGNETOMETERS

The aim of this chapter is to present principles and analytical models, of a Fluxgate magnetometer that uses the Residence Times Difference (RTD) readout strategy.

1.1. Introduction

Fluxgate magnetometers have always been of interest to the technical and scientific communities as practical and convenient sensors for very low magnetic fields measurements.
Fluxgate measure dc or low-frequency ac magnetic fields. They are vector devices, i.e. sensitive to the field direction with achievable resolution of few picotesla. Although Fluxgate sensors are studied since 1930s, these sensors are still being used in many applications.
Recent development of magnetoresistors, especially anisotropic magnetoresistance sensors (AMR) and Giant magnetoresistance (GMR), limit the market for Fluxgate to applications requiring high precision and resolution.
Resolution of 100 pT and 10 nT absolute precision is standard in commercially devices, but they can reach 10 pT resolution and 1 nT long-term stability.
If resolution in the nanotesla range is required, Fluxgates are then the best selection. Compared to high-temperature superconducting

quantum interference device (SQUID) they may have similar noise level, but the measurement range of Fluxgate is much larger.
If picotesla or even smaller fields are measured, a low-temperature SQUID should be used.
Magnetoresistors, mainly anisotropic magnetoresistance sensors, are the main competitors of Fluxgate sensors. Commercially available AMR magnetoresistors such as Philips KMZ have a resolution worse than 10 nT, but they are smaller and cheaper and may consume less energy.

The most frequently used principle of Fluxgate magnetometers is the second-harmonic detection of the output voltage [1.1-1.3].
However, a time domain readout strategy can lead to a set of significant improvement versus the classical 2nd harmonic readout, without loss of performances.
A very simple sensor structure, negligible onboard power requirements and the intrinsic digital form of the readout signal are the main advantages of the proposed strategy, over the conventional Fluxgate operation mode.

1.2. Operating Principle

The structure of a single core RTD Fluxgate magnetometer is schematized in Fig. 1.1: a primary and a secondary coil are wounded around a suitable soft-ferromagnetic core, characterized by a very sharp hysteresis loop and a low coercitive field value (< 20 A/m – Fig. 1.2).

A periodic current (triangular or sinusoidal) is forced through the primary coil, producing the excitation magnetic field $H_E(t)$; the amplitude of this driving current has to be high enough to saturate the core material alternatively in one verse and in the other.

The core magnetization will thus be almost square-shaped and the magnetic flux will follow, in first approximation at least, the magnetization waveform. The output voltage at the secondary coil, being proportional to the magnetic flux, will present a train of bipolar impulses (fig. 1.2).

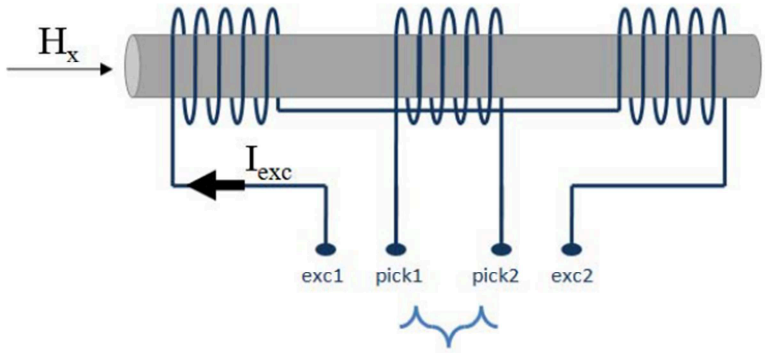

Figure 1.1 – RTD Fluxgate sensor structure

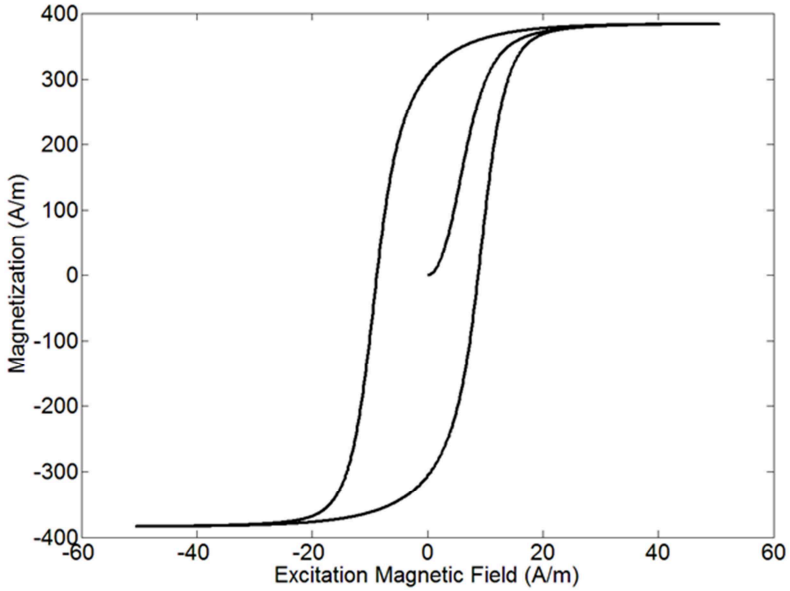

Fig. 1.2 – Typical H-M hysteresis loop for a soft-ferromagnetic core

The shape of these impulses is related to many geometrical and electrical parameters, the most important are the hysteresis shape of the core material and the amplitude and frequency of the driving current.

When the target magnetic field intensity is zero, the time position of these impulses is perfectly regular: for each period (T), we have a positive impulse at $t = 0$ and a negative one at $t = T/2$.

Referring to fig. 3, we define a positive residence time, $T+$ and a negative residence time, $T-$; the Residence Times Difference is thus simply defined as: $RTD = T+ - T-$.

The RTD is taken as the output quantity of the device for convenience. A non-zero target magnetic field acts as an offset applied to the driving signal, this produces an asymmetry in the system dynamics. The impulses in the output voltage are no longer symmetric and the RTD is a non-zero value that is related to the target magnetic field amplitude.

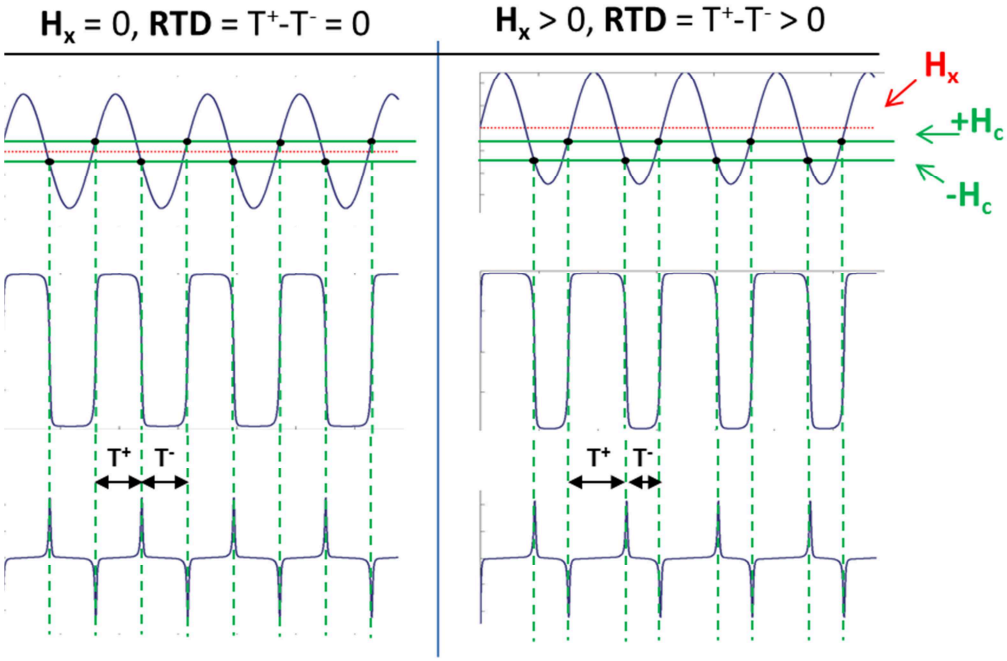

Fig. 1.3 – Top to bottom: the excitation magnetic field, the core magnetization and the output voltage at the secondary coil.

The Residence Times Difference approach has some advantages compared to conventional readout schemes. Chief among them, it can

be implemented experimentally without complicated signal conditioning electronics. In fact, the experimental implementation of this readout scheme requires just one excitation coil and one detection coil without any need of differential structures; it also yields very good results using bias signals having amplitude just sufficient (i.e. barely suprathreshold) to cause switching between the stable states of the hysteretic core with a significant performance improvement from the power budget point of view.

1.2.1. Analytical models of RTD Fluxgate

The $RTD(H_X)$ expression can be derived analytically starting from the definition of the two residence times. However it should be noted that the actual formulation depends on the waveform of the driving current.

As a preliminary consideration it can be noted that, in order to assure an adequate excitation that allows the system to switch between the two saturation states, the amplitude of the excitation field must be large enough to guaranty the crossing of the thresholds (i.e. $\bullet_E > H_C$), nevertheless, thresholds crossing must also be guaranteed in presence of the target hence the target dc field H_X must complain with the following constraint:

$$-\widehat{H}_E + |H_X| < -H_C \Longrightarrow |H_X| < \widehat{H}_E - H_C \tag{1.1}$$

that effectively defines the operating range of the sensor given the operative conditions (the amplitude of the excitation field H_E) and material characteristics (H_C).

1.2.1..1 Sinusoidal driving

We point the attention now to the case of a sinusoidal excitation field of amplitude $\bullet_E$ and frequency $f = 1/T$.
In order to determine an analytic expression for the time interval $RTD = (T+ - T-)$ as function of the field H_X one wishes to detect , the expressions for $T+$ and $T-$ are needed.

Taking into account our definition of the residence times, with reference to Figure 1.3 and 1.4, one immediately obtains the following
equations defining t_1, t_2 and t_3:

$$H_E(t) = \widehat{H}_E \sin(\omega t)$$

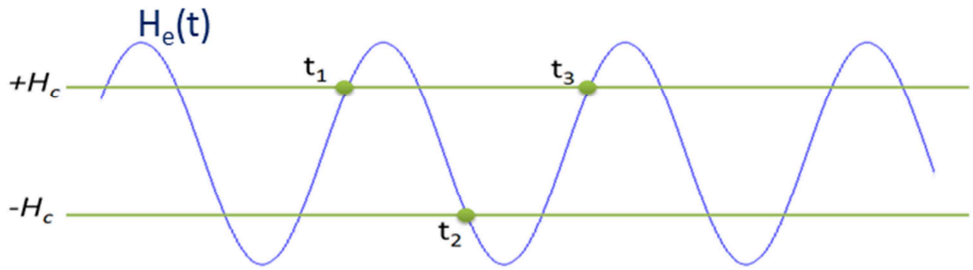

Figure 1.4 – Sinusoidal driving magnetic field.

$$t_1: H_X + H_E(t_1) = H_C \Longrightarrow H_X + \widehat{H}_E \sin(\omega t_1) = H_C$$

$$t_2: H_X + H_E(t_2) = -H_C \Longrightarrow H_X - \widehat{H}_E \sin\left[\omega\left(t_2 - \frac{T}{2}\right)\right] = -H_C$$

$$t_3: t_1 + T$$

$$t_1 = \frac{1}{\omega} arcsin\left(\frac{H_C - H_X}{\widehat{H}_E}\right)$$

$$t_2 = \frac{1}{\omega} arcsin\left(\frac{H_C + H_X}{\widehat{H}_E}\right) + \frac{T}{2}$$

$$t_1 = \frac{1}{\omega} arcsin\left(\frac{H_C - H_X}{\widehat{H}_E}\right) + T$$

The RTD is defined as:

$$RTD = T^+ - T^- = t_2 - t_1 - (t_3 - t_2) = 2t_2 - t_1 - t_3$$

$$RTD = \frac{2}{\omega}\left[arcsin\left(\frac{H_C + H_X}{\widehat{H}_E}\right) - arcsin\left(\frac{H_C - H_X}{\widehat{H}_E}\right)\right]$$

representing the transduction function, RTD versus target magnetic field, H_X valid only in the range defined by the equation (1.1); Figure 1.5 shows the graph of the function.

The analytical expression for the sensitivity is:

$$S = \frac{\partial RTD}{\partial H_X} = \frac{2}{\omega \widehat{H}_E}\left[\frac{1}{\sqrt{1 - \left(\frac{H_C + H_X}{\widehat{H}_E}\right)^2}} + \frac{1}{\sqrt{1 - \left(\frac{H_C - H_X}{\widehat{H}_E}\right)^2}}\right]$$

The nonlinearity of the curve should be noted; however in the small target limit (H_X < 1 A/m) the curve is well approximated by a straight line; sinusoidal bias results then particularly suitable when one wishes to estimate small fields changes, having the possibility to tune the sensitivity at very high value.

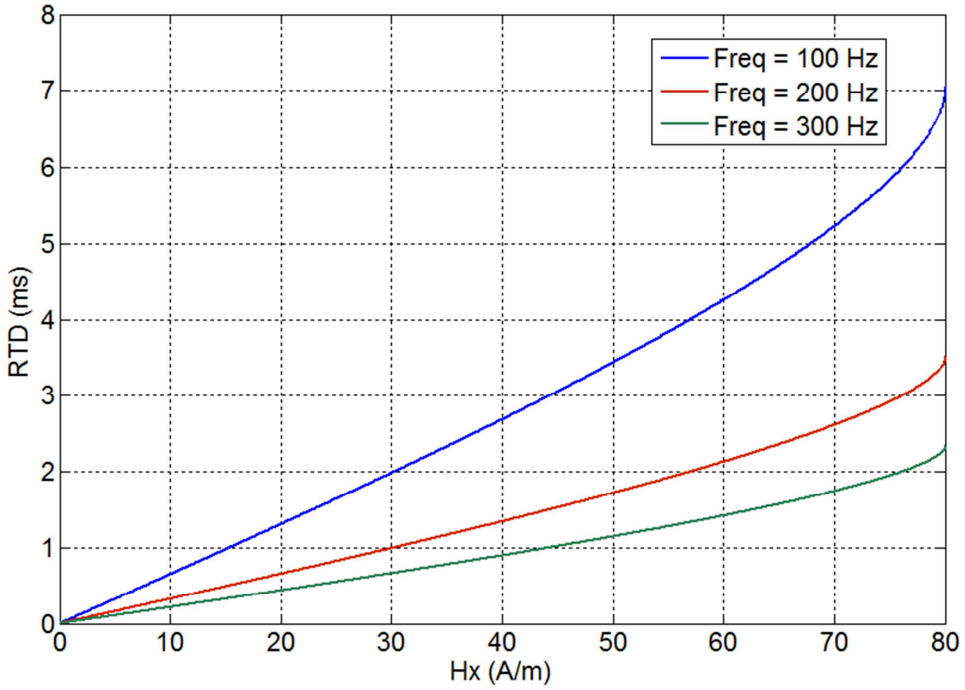

Fig. 1.5 – the transduction function, RTD versus target magnetic field at various frequencies for the driving signal. The situation shown in the figure refers to $\bullet_E$=100 A/m and H_C = 20 A/m

1.2.1..2 Triangular driving

The nonlinearity of the function $RTD(H_X)$, that in some applications may be not desirable, can be overcome by operating the device with a bias field of triangular shape (see Figure 1.6).

A triangular signal, with slope $\bullet$ and period T may be defined as follow:

$$H_e(t) = \begin{cases} \beta t & -\frac{T}{4} \le t \le \frac{T}{4} + NT \\ -\beta t\left(t - \frac{T}{2}\right) & NT + \frac{T}{4} \le t \le \frac{3T}{4} + NT \end{cases}$$

$N = 1,2, \ldots$

The slope • can be expressed as a function of the parameters amplitude and frequency as in the sinusoidal case:

$$\beta = \frac{\widehat{H}_E}{T/4} = \frac{4\widehat{H}_E}{T}$$

In order to determine an analytic expression for the time interval *RTD*, as function of target field the expressions for *T*+ and *T*- are needed; we proceed as in the sinusoidal case, obtaining:

$$t_1 : H_X + \beta t_1 = H_C$$

$$t_1 : H_X - \beta\left(t_2 - \frac{T}{2}\right) = -H_C$$

$$t_3 : t_1 + T$$

whence the residence times *T*+ and *T*- are computed as:

$$T^+ = t_2 - t_1 = \frac{2H_X}{\beta} + \frac{T}{2}$$

$$T^- = t_3 - t_2 = \frac{T}{2} - \frac{2H_X}{\beta}$$

leading to the following expression for the residence times difference RTD:

$$RTD = \frac{4H_X}{\beta}$$

The sensor sensitivity can be finally expressed in the following form:

$$S = \frac{\partial RTD}{\partial H_X} = \frac{4}{\beta} = \frac{1}{f\widehat{H}_E}$$

We observe that, as desired, the sensitivity does not depend on the external magnetic field amplitude and, as the sinusoidal case, inverse proportionality of S respect to frequency and amplitude of the bias is still manifested. Note also that Fluxgate magnetometers actually measure the magnetic field H_x , however the magnetic flux Bx induced in air is conventionally taken to be the measurand. Therefore, in the rest of the work, this latter quantity will be used without invalidating the observations.

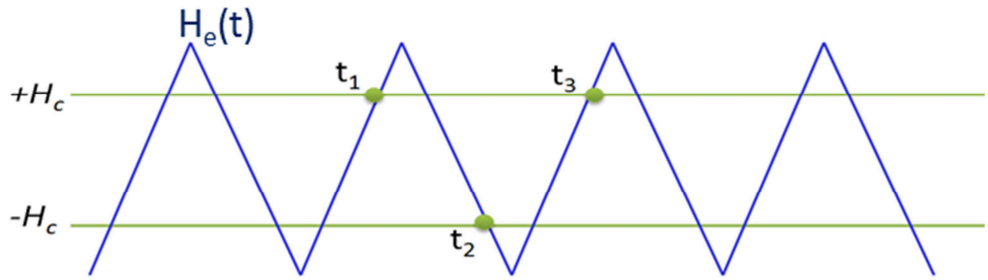

Fig. 1.6 – Triangular driving magnetic field.

1.2.2. A physical model of the RTD Fluxgate

The phenomenological model for the dynamical response of an hysteretic ferromagnetic core can be described by a bistable potential energy function that here follow we will indicate with *U(x)*.
The form of *U(x)* is predicated by micromagnetic phenomena and is usually obtained via mean-field approximations [1.1] to the collective motion of the core domain walls; the form is expressed via the equation:

$$U(x) = \frac{x^2}{2} - \frac{1}{c} ln cos[c(x + H_E(t) + H_X)]$$

This model is used to describe the dynamical behavior of the (normalized) magnetization *x(t)* in the ferromagnetic core via the dynamical system equation [1.2]:

$$\tau \frac{dx}{dt} = -\frac{\partial U(x,t)}{\partial x} = -x + tanh[c(x + H_E(t) + H_X)] \quad (1.2)$$

where H_E represents an excitation periodic field, H_X an external dc magnetic field, independent from H_E, • being the system time constant and c a dimensionless, temperature-dependent, control parameter (the potential function *U(x)* is bi-stable for *c > 1*); this case is shown in Figure 1.7 where the positive and negative stable states are reported in the hysteresis cycle.

In the case of a ferromagnetic core subject to the action of a periodic field H_E, (we assume initially H_X = 0), the magnetization *x(t)* will evolve alternatively from the negative state to the positive state and vice versa, following the hysteretic curve, any time the excitation field exceeds respectively the positive and negative coercive fields H_C and -H_C.

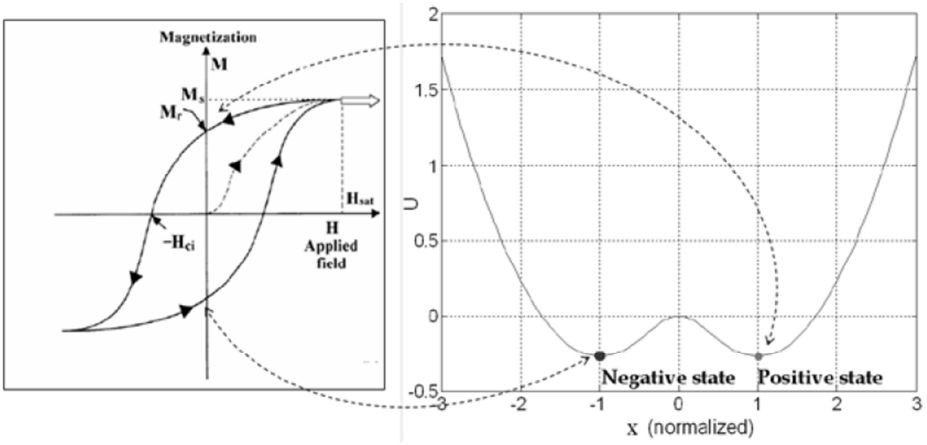

Fig. 1.7 – Relation between the positive and negative stable states of the magnetization dynamic reported in the hysteresis and showed in relation with the potential energy function.

The hypothesis of a very sharp hysteresis of the magnetic core is assumed. This allows us to infer that switching of the magnetization between the two stable states occurs almost instantaneously when the applied magnetic field exceeds the coercive fields level (or thresholds).

In a sense, this is (dynamically) equivalent to the case of strong bias signal situation. Under these conditions, the device operates almost like a static hysteretic nonlinearity, e.g. a Schmitt Trigger. Mathematically, this amounts to the assumption of a very small time-constant • in the mean-field description embodied in (1.2); in fact it is reasonable to assume that, in practice, the signal frequency is smaller than • *-1* , in order for it to significantly affect the system dynamics. Even if this assumption is somewhat violated, however, we can expect to obtain the correct qualitative behavior.

1.3. The Coupled Core Fluxgate Magnetometer

Recently, it has been shown the emergence of oscillations in unforced bistable dynamical systems having dynamics of the general form:

$$\tau\dot{x} = -\nabla_x U(x) \tag{1.3}$$

subject to carefully crafted coupling schemes [6.1]. Here, we present experimental results obtained on a Fluxgate magnetometer that includes $N = 3$ coupled ferromagnetic cores; the oscillatory behavior is triggered when the coupling constant exceeds a threshold value, and the oscillation characteristics are sensitive to an external target dc magnetic signal. Thus the oscillations, which can be induced at frequencies ranging from a few hertz to high-kilohertz, afford a novel detection scheme for dc target magnetic fields. The aim of this work is to describe some features of the coupled sensor system.

1.3.1. The theory of the coupled core Fluxgate Magnetometer

It is well known that unforced systems of the general form (1.3), that represents the general case of system (1.2) used to describe the dynamic of a ferromagnetic core, do not have oscillatory regime.
However, in recent work, it has been demonstrated that coupling N • *3* of elements described by (1.3) in a specific configuration, and en-

suring that the initial state of at least one of them is different from the others, can lead to oscillatory dynamics when a suitably chosen control parameter (either the coupling coefficient or a dc applied signal) exceeds a critical value. The idea of using ferromagnetic systems coupled together to implement this system configuration scheme, clearly, affords the possibility of being able to generate the reference oscillations on-board the ferromagnetic system itself, without the necessity of the externally applied reference signal.

Here we will limit the investigation on a set of $N = 3$ (the required minimal number) coupled systems. The oscillations occur for larger even number N, however, it is still unclear whether there is any practical advantage to increasing N beyond 3. The oscillations can also occur for N very large and even, a situation that has its own rich physics. Accordingly, we will present a theoretical calculations for $N = 3$ noting, however, that the results can easily be generalized to the case of large (but odd) N.

The dynamics of the system are written in the form:

$$\begin{cases} \dot{x}_1 = -x_1 + tanhc(x_1 + \lambda x_2 + \varepsilon) \\ \dot{x}_2 = -x_2 + tanhc(x_2 + \lambda x_3 + \varepsilon) \\ \dot{x}_3 = -x_3 + tanhc(x_3 + \lambda x_1 + \varepsilon) \end{cases} \tag{1.4}$$

Where *xi(t)* represents the (suitably normalized) core magnetization of each unit, and • is the externally applied dc magnetic field (here follow indicated with • to maintain consistent symbolism with references) [1.4]. It is important to note that the oscillatory behavior occurs even for • = *0*, however when • • *0*, the oscillation characteristics change; these changes which might be exploited for signal quantification purposes, are the motivation behind this work.

The elements are assumed to be identical. Notice that the unidirectional coupling term, having strength •, which is assumed to be equal for all three elements, is inside the nonlinearity. The absence of the reference or bias signal (a necessary component of the single Fluxgate setup) in the above equations should also be noted. Again, we reiterate that there are no oscillations for • = *0*.

Under the above conditions, the system displays oscillatory behavior which commences when the coupling coefficient exceeds a threshold value:

$$\lambda_C = -\varepsilon - x_{inf} + \frac{1}{c} tanh^{-1} x_{inf} \qquad (1.4)$$

$$x_{inf} = \sqrt{\frac{c-1}{c}}$$

note that in our convention, • < *0* so that the oscillations occur for |•| > $|•_c|$. The individual oscillations (in each elemental response) are separated in phase by $2•/N$; their temporal characteristics can readily be computed via the theoretical expressions of the positive and negative state Residence Times $T^{\pm}$ of the summed output $\Sigma = \sum_{i=1}^{3} x_i$ that have already been calculated elsewhere [1.5]:

$$T^{+} = \frac{\pi}{\sqrt{c x_{inf}}} \frac{1}{\sqrt{\lambda_C - \lambda}} \qquad (1.5)$$

$$T^{-} = \frac{\pi}{\sqrt{c x_{inf}}} \frac{1}{\sqrt{\lambda_C - \lambda + 2\varepsilon}} \qquad (1.6)$$

whence we can readily write down $T_\Sigma = T^{+} + T^{-}$ for the period of the summed output, and $T_i = N T_\Sigma$ for each individual elemental period [6.1]. The period shows a characteristic dependence on the inverse square root of the bifurcation "distance" $•_c$ - •, as well as the target signal •; these oscillations can be experimentally produced at frequencies ranging from a few hertz to high kilohertz. Note that the oscillations are, actually, switching events between the stable states of each core; they occur as long as at least one element has an initial condition that is different from the remaining elements (clearly, in any practical system with background noise, this condition is easily satisfied). The setup, clearly, eliminates the need to apply the reference bias signal, as required for the single Fluxgate; by generating the oscillations we are, effectively, forcing each core to switch between its stable steady states (the saturation states of its hysteresis loop).

Increasing N changes the frequency of the individual elemental oscillations, but the frequency of the summed response is seen to be independent of N. Figure 1.8 shows the oscillatory behavior obtained via numerical simulations of the coupled core system with the voltage response (proportional to $\dot{x}(t)$) shown in Figure 1.9.

The Residence Times Difference, i.e. the difference in the times spent by the system in its two stable magnetization states, can be computed (for the summed output signal) as $RTD = T^{+} - T^{-}$.

The RTD vanishes (as expected) for •=*0*, and can be used as a quantifier of the target signal, analogous to the time-domain operation of the single Fluxgate. For very small target signals •, we can obtain an approximation to the coupled core RTD [1.5]:

$$RTD \approx \frac{\pi\varepsilon}{\sqrt{cx_{inf}}}(\lambda_{C0} - \lambda)^{-3/2} \qquad (1.7)$$

where $\lambda_{C0} = \lambda_C(\varepsilon = 0)$.

We readily observe that the sensitivity $\bullet RTD/\bullet\bullet$ is significantly enhanced as we get closer to the critical point; this is illustrated in Figure 1.10 and Figure 1.11. Moreover, we note that decreasing the temperature-dependent control parameter c close to unity can also lead to enhanced sensitivity to small •, as is readily apparent in (1.4).

However, for $c < 1$ (corresponding to an increase in the temperature past the Curie point) the system ceases to be bistable and the material becomes paramagnetic. It is worth reiterating that a sensitivity $\bullet T \bullet /\bullet\bullet$,

defined via the (summed) oscillation period, is actually proportional to • (for small •) as can readily be calculated from (1.5) and (1.6). This may not be desirable in practical sensors where one would like to develop the optimal sensor configuration independently of the target signal. Hence, from this standpoint, the *RTD* constitutes the more desirable measure with its sensitivity proportional to the factor $(\lambda_{C0} - \lambda)^{-3/2}$ and independent of •.

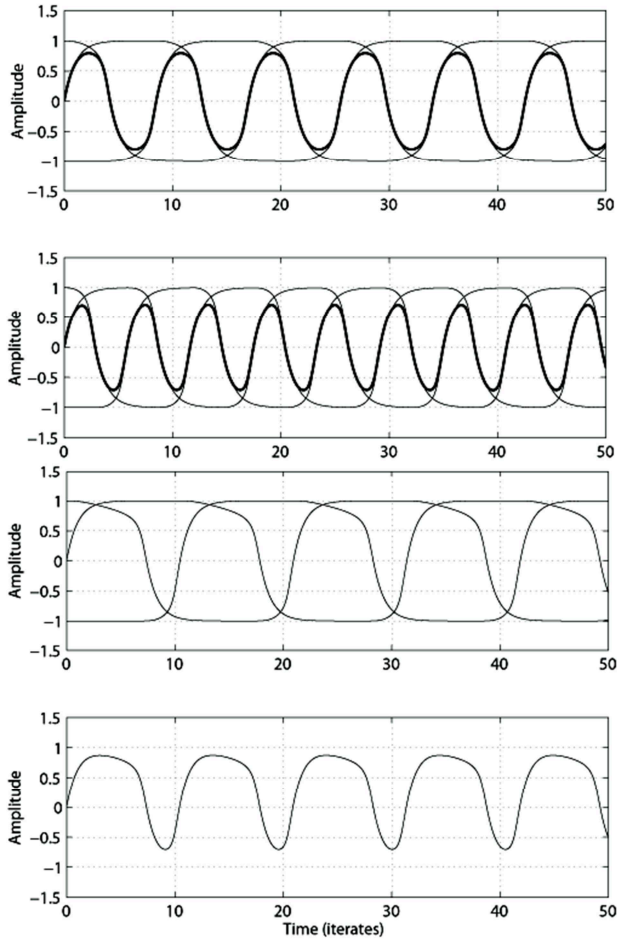

Figure 1.8 - Emergent oscillatory behavior in the coupled core system for $N = 3$. The top panel shows the oscillations near the critical point. Summed response is indicated by thick black lines, and individual element responses follow the grey lines in all panels. The parameters are set at • = -0.60, • = 0. The second panel shows the oscillations for a higher coupling strength • = -0.75, and • = 0; the oscillation frequency increases significantly, scaling as the square root of |•| and •. The third panel shows the individual element oscillations for • = -.60, • = 0.1; the frequency decreases (compared to the top panel) with increasing •. The initial conditions for all simulation runs are (x1 , x2 , x3) = (1.0, 0.0,

-1.0), c = 0.5 , and the time step size is 0.001. For each panel, the critical coupling •, at the onset of the oscillations, may be determined from eq. (1.3)

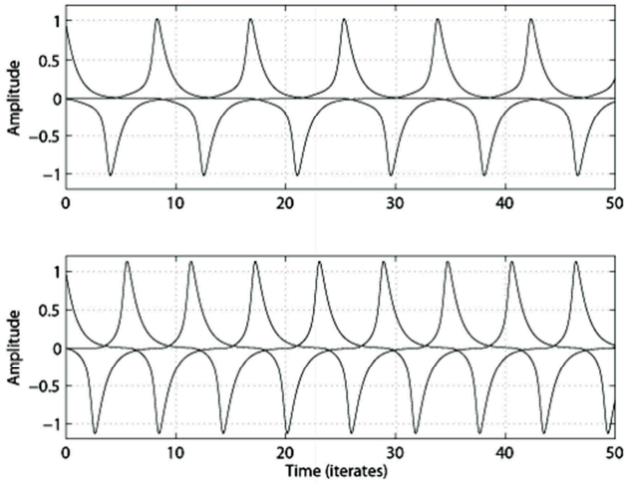

Figure 1.9 - First time derivative (proportional to output voltage) of the state variable *xi(t)* plotted in panel 1 and 2 of Figure 1.8.

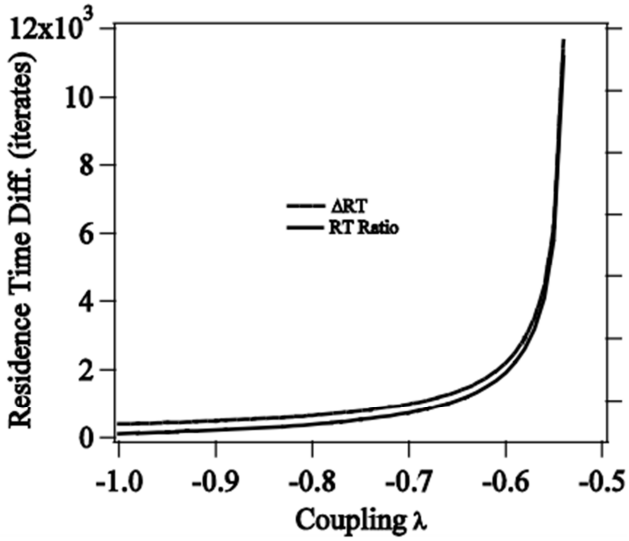

Figure 1.10 - Response curve of the coupled core Fluxgate system to an applied target dc magnetic field • vs. coupling strength. As • approaches the critical value $•_c$ = -0.5345, the response curve rises almost vertically which suggests that the sensitivity of the device increases dramatically in this regime.

c = 3, • = 0.1, and -1.0 << • << -0.54.

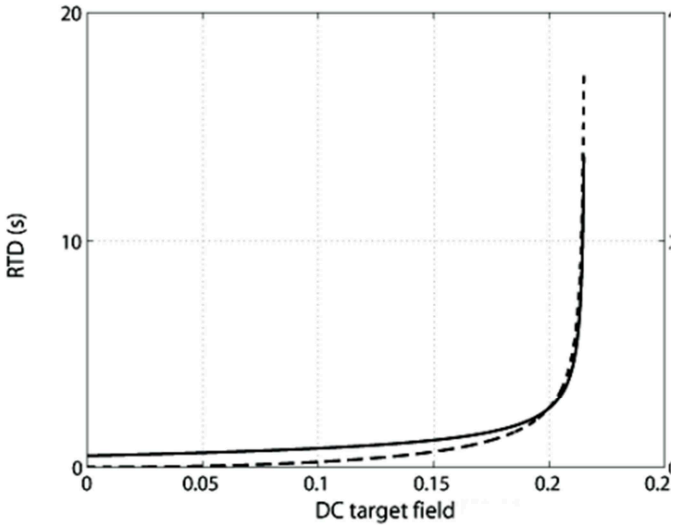

Figure 1.11 - *RTD* plotted as functions of the (weak) dc target signal • with fixed coupling parameter • = -0.8. The sensitivity is now given by the slope of the response curve, and is seen to increase as • approaches the potential energy barrier height of a single (uncoupled) core.

The system sensitivity, defined via the derivative $\bullet RTD/\bullet\bullet$ is found to increase dramatically as one approaches the critical point in the oscillatory regime; this suggests that careful tuning of the coupling parameter so that the oscillations have very low frequency (i.e. just past the critical point of the bifurcation), could offer significant benefits for the detection of very small target signals. This preceding statement must, however, be qualified by an important caveat: in practical setups the oscillation frequency cannot be set too low, in order to ensure good coupling between the cores and the circuit components; in turn, this places an upper bound on the sensitivity.

The absence of the bias signal generator should also result in less system noise, however this must be balanced against the presence of the coupling circuits which require power and will, therefore, contribute to the sensor noise floor.

The (theoretical) results outlined above clearly show that this coupling scheme may allow one to exploit the target-signal dependence of the emergent oscillations for weak (dc) target signal detection and quantification. We now turn to an experimental implementation of both the single core and the coupled core Fluxgate systems; the goal is to describe the experimental results, and the applicability of these kind of magnetometers to real world applications.

REFERENCES

[1.1] F. Forster: A Method for the Measurement of dc Field Differences and its Application to Nondestructive Testing. Nondestruct. Test, vol. 13, pp. 31-41 (1955).

[1.2] F. Primdahl: The Fluxgate Mechanism, Part I: The Gating Curves of Parallel and Orthogonal Fluxgates. IEEE Trans. Magn., vol. 6, issue 2, 376-383 (1970).

[1.3] P. Ripka: Magnetic Sensors and Magnetometers. Artech House, Boston, (2001). the Eddy Current and the Anomalous Losses, Magnetics, IEEE Transactions on, 46 (2010) 3201-3204.

[1.4] A. Bulsara, V. In, A. Kho, P. Longhini, A. Palacios, W.-J. Rappel, J. Acebron, S. Baglio, B. Ando. Phys. Rev. E70, 036103 (2004).

[1.5] V. In, A. Bulsara, A. Palacios, P. Longhini, A. Kho, J. Neff, Phys. Rev., E68, 045102(R) (2003).

[1.6] E. Doedel and X. Wang. Software for Continuation and Bifurcation Problems in Ordinary Differential Equations. Applied Mathematics Report, California Institute of Technology (July 1994).

[1.7] M. Golubitsky, I.N. Stewart, and D.G. Schaeffer. Singularities and Groups in Bifurcation Theory. Appl. Math. Sci. vol. II, Springer-Verlag, New York (1988).

[1.8] D.G. Aronson, M. Golubitsky, and M. Krupa. Nonlinearity, 861 (1991).

[1.9] M. Golubitsky, I. Stewart. Symmetry and Pattern Formation in Coupled Cell Networks, Springer-Verlag, New York (1999).

[1.10] B. Dionne, M. Golubitsky, and I. Stewart, Nonlinearity, 559 (1996).